

基于星载激光雷达与多光谱影像结合的土地覆盖分类方法

黄兴¹, 胡旭嫣², 刘微微³, 赵宏^{4*}

¹丽水市国土空间规划测绘研究院, 浙江 丽水 323000;

²浙南综合工程勘察测绘院有限公司, 浙江 杭州 310030;

³浙江省测绘科学技术研究院, 浙江 杭州 311121;

⁴南京航空航天大学航天学院, 江苏 南京 210016

摘要 针对全波形激光雷达和多光谱数据下土地覆盖误分类问题,提出了融合陆地卫星(Landsat)多光谱遥感影像数据和星载全波形激光雷达全球生态系统动态调查(GEDI)数据进行土地覆盖分类的方法。首先,根据实地调查数据建立数据集;然后,采用支持向量机(SVM)方法来实现激光雷达足迹的土地覆盖分类;最后,对土地覆盖的分类结果进行评价。结果表明,在SVM方法下联合使用光谱特征和波形特征的总体准确率可以达到90.68%,相比仅使用光谱特征或波形特征时总体准确率可以提升8个百分点以上。融合光谱特征和波形特征的方法可以提高土地覆盖分类的准确性。

关键词 测量; 全球生态系统动力学调查; 支持向量机; 土地覆盖分类; Landsat

中图分类号 TP79 文献标志码 A

DOI: 10.3788/CJL231063

1 引言

人类活动会导致土地覆盖类型发生变化,带来了越来越多的生态和环境问题。为有效解决环境问题,进行土地覆盖类型变化监测迫在眉睫^[1-2]。遥感提供了测量大面积地物特征的方法。随着对地观测技术的快速发展,全波形激光雷达以其独特的波形特征,在城区覆盖分类^[3-5]、极地覆盖分类^[6-7]和林业林种分类^[8-11]等方面展现出了巨大优势。

国内外学者针对全波形激光雷达在土地覆盖分类中的应用开展了较多研究。Pirotti^[12]认为波形特征不仅可以提供目标的高度信息,还可以提供目标的一些结构信息。目前,研究人员已经可以利用波形特征来识别特定的土地覆盖类型,例如冰雪^[6-7]、森林^[13-18]、湖泊^[19-20]和城市^[3, 21]。但是已有的研究也表明仅利用波形数据进行分类会存在一些问题,例如:随着地物类别增加,分类准确度会下降;不同类别的地物有着相似的波形特征,从而导致分类精度较差^[13, 16]。为了提高分类的准确率,需要在波形特征中添加辅助特征。已有研究通过将波形特征与光学影像的光谱特征结合起来提高土地覆盖分类的准确率^[22-25],比如,Liu等^[22]将

GLAS与Landsat相结合获得了91%的分类精度。

目前,星载全波形雷达产品主要有NASA的ICESat/GLAS、全球生态系统动力学调查(Global Ecosystem Dynamics Investigation, GEDI)以及国产高分7号卫星。与GEDI相比,GLAS只有2003年至2009年的观测数据,无法用于现在土地覆盖的研究。GEDI的数据始于2019年,可以更好地反映土地覆盖类型的垂直结构,并且其脚印点直径为25 m,可以更好地与Landsat 30 m分辨率的遥感影像匹配。

目前还没有联合使用GEDI足迹的波形属性与光学影像的光谱特征进行土地覆盖分类的研究,因此,将GEDI波形特征与光学影像的光谱特征结合起来对土地覆盖类型进行分类具有积极意义。如果分类精度足够高,可以在难以进行实地调查或无法获取高分辨率遥感图像的地区得到大量的训练/验证样本,从而补充土地覆盖分类任务的样本,进而提高分类的准确度。笔者开发了一种新的土地覆盖分类的方法,该方法集成了GEDI的波形特征和Landsat OLI的光谱特征,同时利用支持向量机(SVM)作为分类器。本文将联合使用GEDI波形特征和光学影像光谱特征的分类结果与单一数据的分类结果进行了对

收稿日期: 2023-07-27; 修回日期: 2023-08-20; 录用日期: 2023-10-09; 网络首发日期: 2023-10-24

基金项目: 自然资源部国土卫星遥感应应用重点实验室开放基金(KLSMNR-K202205)、浙江省基础公益研究计划(LTGS23D010003)、浙江省自然资源厅2023年度自然资源科技项目(2023-20)

通信作者: *nuazhaohong@nuaa.edu.cn

比,以便将所提方法用于在较大区域进行 GEDI 脚印点的分类。

2 研究方法

2.1 GEDI 数据选取与预处理

GEDI 于 2019 年开始工作并得到数据,笔者选取了 2020 年 5 月 1 日至 2020 年 10 月 30 日采集的 L2A 数据。GEDI L2A 数据集经过 6 种不同算法设置的处

理得到了不同的波形特征。本研究提取的参数包括与光斑质量相关的参数(如 quality_flag、degrade_flag、sensitivity 等)、地面高程 elev_lowestmode 和波形特征百分位高度(如 rh0、rh25、rh50、rh75、rh100 等),还有其他相关特征,如高斯分量个数(rx_nummodes)、每个高斯分量的中心位置(rx_modelocs)、每个高斯分量的宽度(rx_modewidths)等。具体参数如表 1 所示。

表 1 GEDI L2A 提取参数列表
Table 1 GEDI L2A extraction parameters list

Variable name	Range of data values	Description
quality_flag	0, 1	Quality identification
degrade_flag	0, 1	Quality identification
sensitivity	0-1	Sensitivity
lon_lowestmode	118°-123°	Longitude
lat_lowestmode	27°-32°	Latitude
elev_lowestmode	0-2000 m	Ground elevation
elev_highestreturn	0-50 m	Crown elevation
digital_elevation_mode_srtm	0-2000 m	SRTM elevation
Rh(0, 25, 50, 75, 100)	-10-40 m	Percentile height
rx_nummodes		Number of modes detected in waveform
lastmodeenergy		Energy in lowest detected mode
smoothwidth		Width of Gaussian function used to smooth noise sections of waveforms
rx_modelocs		Sample numbers of each detected mode (relative to bin 0 of waveform)
rx_modewidths		1 sigma width estimates of each detected mode in waveform
peak		Peak amplitude of raw waveform
pk_sm		Peak amplitude of smoothed waveform

GEDI L2A 包含了数据质量判断参数(如质量标志参数 quality_flag)、灵敏度参数(sensitivity)等,可以使用这些标志参数剔除每种算法设置中地理定位精度差的光斑、信号质量差的波形以及受云和其他地表条件影响的无效光斑,保留每种算法设置中质量较好的

GEDI 光斑。为了获取研究区内高质量的 GEDI 光斑,首先用 GEDI L2A 的经纬度 lon_lowestmode、lat_lowestmode 选出研究区内的 GEDI 光斑,然后用 GEDI L2A 数据包含的质量相关参数剔除部分无效 GEDI 光斑。具体筛选条件如表 2 所示。

表 2 GEDI L2A 有效足迹筛选条件
Table 2 GEDI L2A valid footprint screening conditions

Screening parameter	Screening condition	Instruction
degrade_flag	0	The state degradation flag is "1", indicating that the state of the indicating direction and/or positioning information decreases, which affects the accuracy of the GEDI L2A data. Therefore, the light spot with the value of 1 is deleted
sensitivity	≥0.95	Sensitivity parameter: on land, a sensitivity threshold greater than or equal to 0.9 is used to obtain better quality light spots, so the light spots with sensitivity less than 0.95 are deleted
quality_flag	1	A quality mark of "1" indicates that the waveform meets specific criteria based on energy, sensitivity, amplitude, and real-time surface tracking quality and can be represented as a valid waveform
elev_lowestmode-SRTM	≤50	Because GEDI is susceptible to the influence of clouds in the data collection, delete the light spot whose elev_lowestmode value is significantly different from the SRTM value of the GEDI footprint (elev_lowestmode-SRTM >50 m)
rx_assess_flag	0	If the value is 1, various errors may occur in the waveform. Therefore, the light spot of rx_assess_flag=1 is deleted

2.2 Landsat 特征选取

Landsat 光谱数据来自 Google Earth Engine 数据库中的 USGS Landsat 8 Surface Reflectance Tier 1 数据集,采集时间为 2020 年 1 月 1 日至 2020 年 12 月 31 日,采用的波段信息如表 3 所示。利用 GEE 平台对数据进行操作,利用 Cfmask 算法生成的 QA 数据去除每幅图像中被云污染的像素,再将全部的多光谱数据取中位数作为全年的光谱数据。

表 3 Landsat 光谱波段的基本信息
Table 3 Basic information of Landsat spectral band

Band	Resolution /m	Wavelength /nm	Description
B2	30	452-512	Blue
B3	30	533-590	Green
B4	30	636-673	Red
B5	30	851-879	Near infrared
B6	30	1566-1651	Shortwave infrared 1
B7	30	2107-2294	Shortwave infrared 2

光谱特征除遥感影像原始波段以外还有多个光谱指数,如归一化植被指数(NDVI,在公式中记为 ζ_{NDVI})、归一化差异水体指数(NDWI,在公式中记为 ζ_{NDWI})、归一化建筑指数(NDBI,在公式中记为 ζ_{NDBI})、增强型植被指数(EVI,在公式中记为 ζ_{EVI})、比值植被指数(RVI,在公式中记为 ζ_{RVI})、大气阻抗植被指数(ARVI,在公式中记为 ζ_{ARVI})。植被指数的具体计算公式如表 4 所示,其中, ρ_{NIR} 表示近红外波段的反射率, ρ_{RED} 表示红光波段的反射率, ρ_{SNIR} 表示短波红外波段的反射率, ρ_{GREEN} 表示绿光波段的反射率, ρ_{BLUE} 表示蓝光波段的反射率。

表 4 植被指数
Table 4 Spectral vegetation index

Vegetation index	Equation
NDVI	$\zeta_{\text{NDVI}} = \frac{\rho_{\text{NIR}} - \rho_{\text{RED}}}{\rho_{\text{NIR}} + \rho_{\text{RED}}}$
NDBI	$\zeta_{\text{NDBI}} = \frac{\rho_{\text{SNIR}} - \rho_{\text{NIR}}}{\rho_{\text{SNIR}} + \rho_{\text{NIR}}}$
NDWI	$\zeta_{\text{NDWI}} = \frac{\rho_{\text{GREEN}} - \rho_{\text{NIR}}}{\rho_{\text{GREEN}} + \rho_{\text{NIR}}}$
ARVI	$\zeta_{\text{ARVI}} = \frac{\rho_{\text{NIR}} - (2\rho_{\text{RED}} - \rho_{\text{BLUE}})}{\rho_{\text{NIR}} + (2\rho_{\text{RED}} - \rho_{\text{BLUE}})}$
EVI	$\zeta_{\text{EVI}} = 2.5 \left(\frac{\rho_{\text{NIR}} - \rho_{\text{RED}}}{\rho_{\text{NIR}} + 6\rho_{\text{RED}} - 7.5\rho_{\text{BLUE}} + 1} \right)$
RVI	$\zeta_{\text{RVI}} = \frac{\rho_{\text{NIR}}}{\rho_{\text{RED}}}$

2.3 支持向量机

支持向量机(SVM)是建立在统计学习理论基础上的数据挖掘方法,能非常有效地处理分类问题^[26-28]。SVM不要求数据符合高斯分布,其优点是只要求少的训练样本,而且可以处理高维数据(即特征数多的数据),对过拟合现象不敏感。

SVM分类器的目标是找到一个最优的线性超平面,使两类训练样本尽可能分开,如图 1 所示。

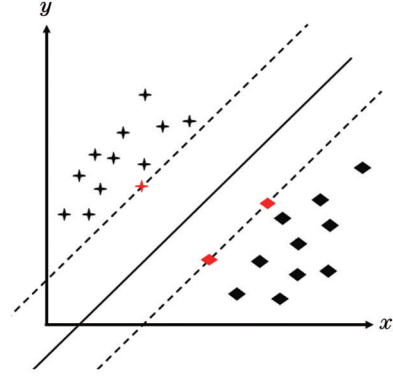


图 1 SVM 算法的原理

Fig. 1 Support vector machine (SVM) algorithm principle

SVM 借助二次规划问题来求解支持向量,即

$$\min_{\omega, \xi, b} \left\{ \frac{1}{2} \|\omega\|^2 + C \sum_i \xi_i \right\}, \quad (1)$$

式中: C 为惩罚系数,用来控制分类器的归一化能力,由用户选择; ξ_i 是松弛变量,用来控制允许的误差; ω 为超平面的法向量; b 为超平面的截距。实际上,存在很多线性不可分的情况,对这些无法进行线性分划的样本,需要将原始训练点映射到 Hilbert 空间后再进行线性分划,然后再把分划直线变换到原始空间上。这里的映射以内积的形式存在,并通过核函数实现。本文采用径向基核函数 RBF,其表达式为

$$K(\mathbf{x}, \mathbf{y}) = \exp\left(-\gamma \|\mathbf{x} - \mathbf{y}\|^2\right), \quad \gamma > 0, \quad (2)$$

式中: γ 为核参数。

2.4 基于 SVM 的脚印点分类模型

本文构建的 SVM 脚印点分类模型的具体分类流程如下所述:

步骤 1:提取研究区内 2020 年的 GEDI L2A 脚印点,然后利用调查数据对脚印点下的地物类别进行标注,同时提取脚印点处的 Landsat 遥感影像的光谱反射率,并计算植被指数。

步骤 2:将脚印点处的波形信息和光谱作归一化处理,并将样本数据随机划分为训练数据集和验证数据集,其中 70% 的训练数据用于训练 SVM 分类模型,剩下的 30% 用于验证分类模型的精度。

步骤 3:将训练数据集中的特征向量输入到 SVM 分类模型,使用 GridSearchCV 对 SVM 的惩罚系数和核函数进行搜索得到最优参数并训练构建脚印点最优

分类模型。

步骤 4: 利用验证数据集计算生产者准确性 (PA)、用户准确性 (UA)、总体准确率 (OA) 和 Kappa 系数, 用这些参数对模型进行评价。

步骤 5: 提取研究区 6 个子区域内的样本数据, 基于每个区域内的数据训练模型, 预测其他区域的分类结果, 对所提方法的适用性进行评价。

3 分析与讨论

3.1 样本筛选结果

经过处理和筛选后样本总数为 2902 个, 样本分布情况如图 2 所示。在每个类别中, 样本分为训练样本和验证样本, 训练样本占每个类别样本的 70%, 它们从样本集中随机抽取, 每个类别中的剩余样本用作验证样本 (表 5)。选择 6 个子区域, 提取子区域内的实地调查数据。此外, 添加部分目视解译数据进行方法适用性检验。

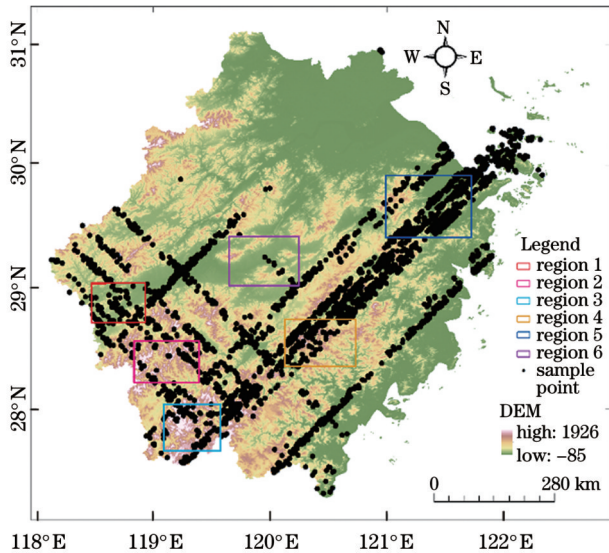


图 2 研究区样点分布

Fig. 2 Sample site distribution in the study area

表 5 各土地覆盖类别的样本数

Table 5 Sample size for each land cover category

Land cover category	Sample count	Training sample count	Validation sample count
Forest	529	375	154
Shrubland	465	316	149
Grassland	502	350	152
Cropland	464	318	146
Water	456	328	128
Others	486	350	136

为了消除特征之间的量纲影响, 同时为了解决数据特征之间的可比性, 需要对数据进行标准化处理。

经过数据标准化处理后, 各指标处于同一数量级, 适合进行综合对比。利用式 (3) 将特征的数值范围缩放到 -1 到 1 之间^[22]。

$$y = \frac{(y_{\max} - y_{\min})(x - x_{\min})}{x_{\max} - x_{\min}} + y_{\min}, \quad (3)$$

式中: x 是原始值; y 是缩放后的值; x_{\min} 和 x_{\max} 分别是原始数据的最小值和最大值; y_{\min} 和 y_{\max} 的值分别是 -1 和 1。

3.2 特征选择

笔者计算了两类源变量 (波形和光谱) 对一般分类模型的重要性。图 3 给出了所有特征 (63 个) 对于一般分类的重要性, 其中: 最相关的波形特征是 GEDI 数据中的 rx_nummodes 以及 rx_modewidths 和 rx_modelocs 中的部分特征, 而 rx_modewidths 和 rx_modelocs 中的其他特征对于分类并没有帮助; 特别相关的光谱特征来自与近红外、红光波段相关的植被指数 NDVI、RVI 和 DVI 等。基于特征重要性的排序, 选择 20 个特征,

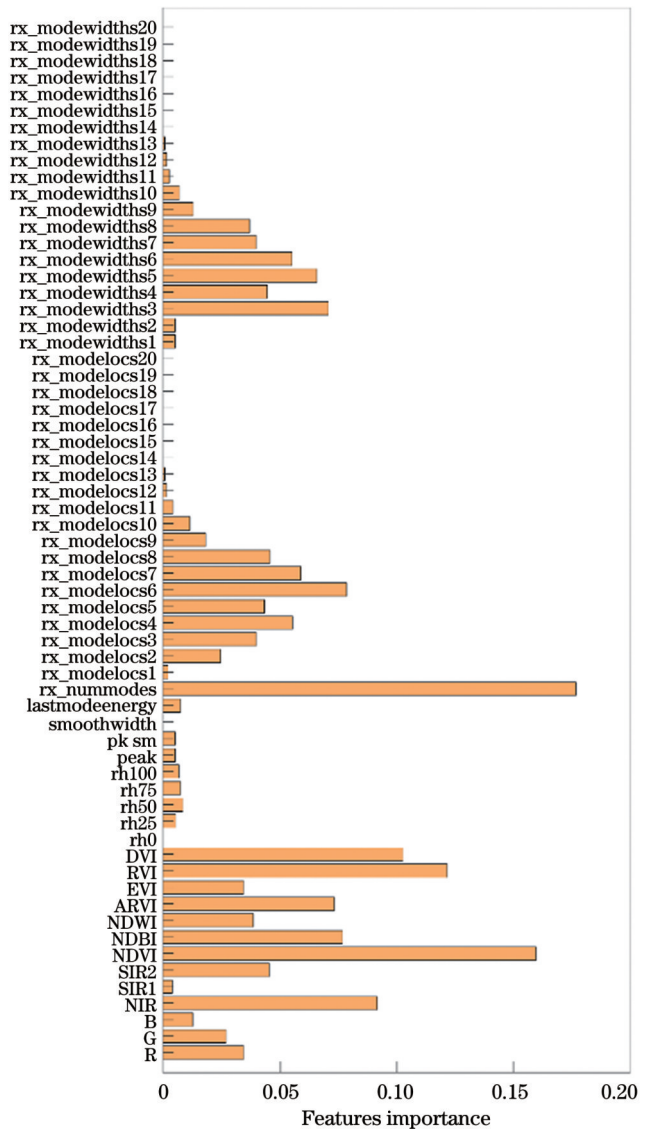


图 3 特征重要性

Fig. 3 Importance of different features

分别为 NDVI、DVI、RVI、rx_nummodes、NIR、ARVI、NDBI、R、SIR2、rx_modelocs6、rx_modelocs8、rx_modewidth5、rx_modewidth6、rx_modelocs7、NDWI、rx_modewidth8、rx_modewidth3、rx_modewidth7、G 和 EVI,用于模型训练。

3.3 土地覆盖分类结果与分析

将光谱特征和波形特征以各种组合进行分组,如表 6 所示。计算混淆矩阵并将计算结果列于表 7~11。由表 7~11 可知,联合使用光谱特征和波形特征比单独使用光谱或波形特征的分类精度要高,仅使用一种类型特征时的 OA 均低于 82%,但协同使用时的 OA 可以达到 90% 以上。表 12 给出了每个区域的样本数量,表 13 给出了子区域预测结果的 OA。表 13 显示,6 个子区域内的 OA 也可以达到 83% 以上,证明了所提

表 6 不同的特征组

Table 6 Different groups of features

Feature group number	A feature group contains features
1	All waveform features (47)
2	All spectral features (13)
3	Selected waveform features (9)
4	Selected spectral features (11)
5	Selected waveform and spectral features (20)
6	Selected regions sample (6 regions)

方法具有普遍适用性。联合使用光谱特征和波形特征可以有效区分具有相似光谱特征或垂直特征的地物。

表 7 特征组 1 的混淆矩阵

Table 7 Confusion matrix of feature group 1

SVM	Ground reality data						UA / %	Kappa	OA / %
	Forest	Shrubland	Grassland	Cropland	Water	Others			
Forest	96	20	15	12	9	2	62.34	0.59	65.10
Shrubland	38	78	17	5	4	7	52.35		
Grassland	35	15	84	12	3	3	55.26		
Cropland	8	8	10	102	4	20	67.11		
Water	4	1	7	2	111	3	86.72		
Others	9	3	3	15	10	96	70.59		
PA / %	50.53	62.40	61.76	68.92	78.72	73.28			

表 8 特征组 2 的混淆矩阵

Table 8 Confusion matrix of feature group 2

SVM	Ground reality data						UA / %	Kappa	OA / %
	Forest	Shrubland	Grassland	Cropland	Water	Others			
Forest	134	0	1	0	1	18	87.01	0.75	78.825
Shrubland	15	91	20	18	2	3	61.07		
Grassland	8	9	127	8	0	0	83.55		
Cropland	11	5	36	91	0	3	62.33		
Water	1	0	1	0	123	3	96.09		
Others	13	2	2	2	3	114	83.82		
PA / %	73.63	85.05	67.91	76.47	95.35	80.85			

表 9 特征组 3 的混淆矩阵

Table 9 Confusion matrix of feature group 3

SVM	Ground reality data						UA / %	Kappa	OA / %
	Forest	Shrubland	Grassland	Cropland	Water	Others			
Forest	120	19	7	2	3	3	77.92	0.68	72.90
Shrubland	23	84	25	9	2	6	56.38		
Grassland	15	20	94	8	5	10	61.84		
Cropland	2	6	12	108	3	21	71.05		
Water	2	3	2	4	116	1	90.63		
Others	7	7	2	4	3	113	83.09		
PA / %	71.01	60.43	66.20	80.00	87.88	73.38			

表 10 特征组 4 的混淆矩阵
Table 10 Confusion matrix of feature group 4

SVM	Ground reality data						UA / %	Kappa	OA / %
	Forest	Shrubland	Grassland	Cropland	Water	Others			
Forest	136	1	0	1	0	16	88.31	0.79	81.75
Shrubland	13	100	17	16	1	2	67.11		
Grassland	5	8	130	9	0	0	85.53		
Cropland	9	4	30	107	0	2	70.39		
Water	1	0	1	0	126	0	98.44		
Others	13	2	3	1	4	113	83.09		
PA / %	76.84	86.96	71.82	79.85	96.18	84.96			

表 11 特征组 5 的混淆矩阵
Table 11 Confusion matrix of feature group 5

SVM	Ground reality data						UA / %	Kappa	OA / %
	Forest	Shrubland	Grassland	Cropland	Water	Others			
Forest	143	6	0	2	0	3	92.86	0.89	90.68
Shrubland	13	126	4	6	0	0	84.56		
Grassland	5	8	134	4	0	1	88.16		
Cropland	1	6	6	137	0	0	91.33		
Water	2	0	0	1	122	3	95.31		
Others	3	2	1	2	2	126	92.65		
PA / %	85.63	85.14	92.41	90.13	98.39	94.74			

表 12 子区域内土地覆盖类别的样本数量
Table 12 The number of samples of land cover categories in the subregion

Category	The number of samples					
	Region 1	Region 2	Region 3	Region 4	Region 5	Region 6
Forest	100	99	105	103	99	99
Shrubland	61	93	96	103	105	28
Grassland	98	103	99	102	102	53
Cropland	102	97	95	98	98	95
Water	104	3	32	59	104	66
Others	95	26	95	103	96	97

表 13 子区域预测结果的 OA
Table 13 The overall accuracy of sub-region prediction results

Model	OA / %					
	Region 1	Region 2	Region 3	Region 4	Region 5	Region 6
Region 1 model	88.50	86.29	84.23	84.39	86.44	87.04
Region 2 model	85.50	87.27	85.29	86.69	84.39	86.65
Region 3 model	85.43	84.21	85.96	84.93	83.89	83.31
Region 4 model	84.25	83.01	85.25	86.97	84.70	83.19
Region 5 model	87.71	85.84	83.52	83.41	88.54	86.24
Region 6 model	87.35	84.41	86.31	85.28	85.42	89.21

对比表 8 与表 10、表 9 与表 11 的分类结果可知,特征组 4、5 的各评价指标均有提升,这说明分类时特征选择对于 SVM 的性能很重要。由于地形等因素的影响,复杂地形区域森林、灌丛、农田的波形特征相近,因此在仅使用波形时会出现错分的情况。当仅使用光谱时,由于森林、灌丛、草地和农田的光谱特征相近,也会出现误分类的情况。此外,有 16~18 个森林样本被分入其他类中,其原因可能是森林区域内的地形影像有阴影,导致光学影像无法获取到地物的有效光谱而错分。其他类被误分为森林可能是因为这些类中的脚印点所在区域包含城镇绿地,导致地物反射率中包含植被的反射率,从而导致了错分。使用光谱特征进行水识别总是比单独使用波形特征具有更高的 UA 和 PA,这说明光谱特征是水的主要特征。

为了验证所提方法的适用性,选择研究区内 6 块子区域(包含平原、山地和丘陵地貌)的实地调查数据进行模型训练和模型结果验证。由于实地调查点数量有限,因此采取目视识别的方式补充部分样点,但在某些区域一些地物的样点数量依然偏少,每个区域样本数如表 12 所示。利用每个区域的模型去预测其他区域的分类结果,预测结果如表 13 所示,6 个区域模型的准确度在 85.96%~89.21% 之间,准确率较高。其余各区域的预测结果在 83.01%~87.71% 之间,与模型本身准确率相差在 5% 之内,具有较高的准确率。此结果可以说明所提方法具有比较可靠的适用性,模型准确率下降的原因可能是类别不均衡和样本总数少导致的。

4 结 论

本文提出了一种融合多光谱遥感影像数据和星载全波形激光雷达数据进行土地覆盖分类的方法,该方法通过联合 Landsat 光谱数据的光谱特征和 GEDI 全波形激光雷达数据的波形数据来提高土地覆盖分类预测的准确性。光谱特征和波形特征联合使用时的 OA 为 90.68%,相比使用单一特征时的 OA 至少可以提升 8 个百分点。当地物的光谱特征相似时,波形特征提供的结构信息在区分不同的土地覆盖类型方面起着重要作用,同样,当出现具有不同结构特性的同类型物体或具有相同结构特性的不同类型物体时,光谱特征起关键作用。此外,本文利用数据集中 6 个子区域的数据进行了测试模型适用能力的检验,结果表明所提方法具有较好的普遍适用性。因此,联合使用来自 GEDI 和 Landsat OLI 数据的高度和光谱特征有利于 GEDI 足迹的土地覆盖分类。

此外,GEDI L2A 包含的数据特征来自原始波形处理后的结果,如果直接使用 L1B 的原始波形或者经过处理后得到的波形特征,对于提升分类的准确度可能会有较大帮助,并且添加地物的结构特征后可能会实现对森林中具体树种的精准分类。因为实地调查获

取的数据较少,而且这些数据在空间上呈非均匀分布,在进行方法适用性测试时需要划分为多个区域,导致每个区域内的样本数量少且类别数不均衡,进而导致模型准确率有所下降。如果增加每个区域内的样本数量并且平衡每个类别的样本数,则在验证区域可能会获得更优的实验结果。

参 考 文 献

- [1] Abbasi M K, Zafar M, Khan S R. Influence of different land-cover types on the changes of selected soil properties in the mountain region of Rawalakot Azad Jammu and Kashmir[J]. *Nutrient Cycling in Agroecosystems*, 2007, 78(1): 97-110.
- [2] Dallmeyer A, Claussen M. The influence of land cover change in the Asian monsoon region on present-day and mid-Holocene climate[J]. *Biogeosciences*, 2011, 8(6): 1499-1519.
- [3] Cheng F, Wang C, Wang J L, et al. Trend analysis of building height and total floor space in Beijing, China using ICESat/GLAS data[J]. *International Journal of Remote Sensing*, 2011, 32(23): 8823-8835.
- [4] Mallet C, Soergel U, Bretar F. Analysis of full-waveform lidar data for classification of urban areas[EB/OL]. [2023-03-05]. https://www.ipi.uni-hannover.de/uploads/tx_tkpublikationen/Mallet_Peking_2008.pdf.
- [5] Mallet C, Bretar F, Roux M, et al. Relevance assessment of full-waveform lidar data for urban area classification[J]. *ISPRS Journal of Photogrammetry and Remote Sensing*, 2011, 66(6): S71-S84.
- [6] Molijn R A, Lindenbergh R C, Gunter B C. ICESat laser full waveform analysis for the classification of land cover types over the cryosphere[J]. *International Journal of Remote Sensing*, 2011, 32(23): 8799-8822.
- [7] 谭继强, 詹庆明, 韩凉, 等. ICESat GLAS 完整波形信号处理技术在南极查尔斯王子山脉地区地表覆盖分类中的应用研究[J]. *测绘与空间地理信息*, 2016, 39(4): 8-12.
Tan J Q, Zhan Q M, Han L, et al. ICESat/GLAS full waveform signal processing for land cover classification in Antarctica prince Charles Mountains[J]. *Geomatics & Spatial Information Technology*, 2016, 39(4): 8-12.
- [8] Nelson R, Ranson K J, Sun G, et al. Estimating Siberian timber volume using MODIS and ICESat/GLAS[J]. *Remote Sensing of Environment*, 2009, 113(3): 691-701.
- [9] Yao W, Krzystek P, Heurich M. Tree species classification and estimation of stem volume and DBH based on single tree extraction by exploiting airborne full-waveform LiDAR data[J]. *Remote Sensing of Environment*, 2012, 123: 368-380.
- [10] Neuenschwander A L, Magruder L A, Tyler M. Landcover classification of small-footprint, full-waveform lidar data[J]. *Journal of Applied Remote Sensing*, 2009, 3(1): 033544.
- [11] Fieber K D, Davenport I J, Ferryman J M, et al. Analysis of full-waveform LiDAR data for classification of an orange orchard scene [J]. *ISPRS Journal of Photogrammetry and Remote Sensing*, 2013, 82: 63-82.
- [12] Pirotti F. IceSAT/GLAS waveform signal processing for ground cover classification: state of the art[J]. *Italian Journal of Remote Sensing*, 2010, 42(2): 13-26.
- [13] Duong H, Pfeifer N, Lindenbergh R. Full waveform analysis: ICESat laser data for land cover classification[J]. *International Archives of Photogrammetry, Remote Sensing and Spatial Information Sciences*, 2006, 36(7): 30-35.
- [14] Cheng X. Waveform-based classification of medium-footpoint LVIS data[C]//13th International Conference on Lidar Applications for Assessing Forest Ecosystems, October 9, 2012, Beijing, China. [S.l.:s.n.], 2013:9-17.
- [15] 陈向宇, 云挺, 薛联凤, 等. 基于激光雷达点云数据的树种分类[J]. *激光与光电子学进展*, 2019, 56(12): 122801.

- Chen X Y, Yun T, Xue L F, et al. Classification of tree species based on LiDAR point cloud data[J]. *Laser & Optoelectronics Progress*, 2019, 56(12): 122801.
- [16] Ghosh S, Nandy S, Patra S, et al. Land cover classification using ICESat/GLAS full waveform data[J]. *Journal of the Indian Society of Remote Sensing*, 2017, 45(2): 327-335.
- [17] 陈博文, 史硕, 龚威, 等. 基于空谱特征优化选择的高光谱激光雷达地物分类[J]. *光学学报*, 2023, 43(12): 1228008.
Chen B W, Shi S, Gong W, et al. Target classification of hyperspectral lidar based on optimization selection of spatial-spectral features[J]. *Acta Optica Sinica*, 2023, 43(12): 1228008.
- [18] 卢晓艺, 云挺, 薛联凤, 等. 基于树木激光点云的有效特征抽取与识别方法[J]. *中国激光*, 2019, 46(5): 0510002.
Lu X Y, Yun T, Xue L F, et al. Effective feature extraction and identification method based on tree laser point cloud[J]. *Chinese Journal of Lasers*, 2019, 46(5): 0510002.
- [19] Wang X W, Cheng X, Li Z, et al. Lake water footprint identification from time-series ICESat/GLAS data[J]. *IEEE Geoscience and Remote Sensing Letters*, 2012, 9(3): 333-337.
- [20] Wang X W, Gong P, Zhao Y Y, et al. Water-level changes in China's large lakes determined from ICESat/GLAS data[J]. *Remote Sensing of Environment*, 2013, 132: 131-144.
- [21] Gong P, Li Z, Huang H B, et al. ICESat GLAS data for urban environment monitoring[J]. *IEEE Transactions on Geoscience and Remote Sensing*, 2011, 49(3): 1158-1172.
- [22] Liu C X, Huang H B, Gong P, et al. Joint use of ICESat/GLAS and Landsat data in land cover classification: a case study in Henan Province, China[J]. *IEEE Journal of Selected Topics in Applied Earth Observations and Remote Sensing*, 2015, 8(2): 511-522.
- [23] Ranson K J, Sun G, Kovacs K, et al. Landcover attributes from ICESat GLAS data in Central Siberia[C]//IGARSS 2004.2004 IEEE International Geoscience and Remote Sensing Symposium, September 20-24, 2004, Anchorage, AK, USA. New York: IEEE Press, 2004: 753-756.
- [24] 周梦维, 柳钦火, 刘强, 等. 全波形激光雷达和航空影像联合的地物分类[J]. *遥感技术与应用*, 2010, 25(6): 821-827.
Zhou M W, Liu Q H, Liu Q, et al. A method for classification by fusing full-waveform airborne laser scanning data and aerial images [J]. *Remote Sensing Technology and Application*, 2010, 25(6): 821-827.
- [25] 张爱武, 董喆, 康孝岩. 基于XGBoost的机载激光雷达与高光谱影像结合的特征选择算法[J]. *中国激光*, 2019, 46(4): 0404003.
Zhang A W, Dong Z, Kang X Y. Feature selection algorithms of airborne LiDAR combined with hyperspectral images based on XGBoost[J]. *Chinese Journal of Lasers*, 2019, 46(4): 0404003.
- [26] 王小龙, 闫浩文, 周亮, 等. 利用SVM分类Landsat影像的朝鲜主要城市建设用地时空特征分析[J]. *国土资源遥感*, 2020, 32(4): 163-171.
Wang X L, Yan H W, Zhou L, et al. Using SVM classify Landsat image to analyze the spatial and temporal characteristics of main urban expansion analysis in Democratic People's Republic of Korea[J]. *Remote Sensing for Land & Resources*, 2020, 32(4): 163-171.
- [27] 刘立新, 何迪, 李梦珠, 等. 基于高光谱技术与机器学习的新疆红枣品种鉴别[J]. *中国激光*, 2020, 47(11): 1111002.
Liu L X, He D, Li M Z, et al. Identification of Xinjiang jujube varieties based on hyperspectral technique and machine learning[J]. *Chinese Journal of Lasers*, 2020, 47(11): 1111002.
- [28] 胡海瑛, 惠振阳, 李娜. 基于多基元特征向量融合的机载LiDAR点云分类[J]. *中国激光*, 2020, 47(8): 0810002.
Hu H Y, Hui Z Y, Li N. Airborne LiDAR point cloud classification based on multiple-entity eigenvector fusion[J]. *Chinese Journal of Lasers*, 2020, 47(8): 0810002.
- [29] 张爱武, 董喆, 康孝岩. 基于XGBoost的机载激光雷达与高光谱影像结合的特征选择算法[J]. *中国激光*, 2019, 46(4): 0404003.
Zhang A W, Dong Z, Kang X Y. Feature selection algorithms of airborne LiDAR combined with hyperspectral images based on XGBoost[J]. *Chinese Journal of Lasers*, 2019, 46(4): 0404003.

Land Cover Classification Method Integrating Spaceborne LiDAR Combined with Multispectral Images

Huang Xing¹, Hu Xuyan², Liu Weiwei³, Zhao Hong^{4*}

¹Lishui Institute of Territorial Spatial Planning and Mapping, Lishui 323000, Zhejiang, China;

²Zhejiang South Comprehensive Engineering Survey and Mapping Institute Co., Hangzhou 310030, Zhejiang, China;

³Zhejiang Academy of Surveying and Mapping Science and Technology, Hangzhou 311121, Zhejiang, China;

⁴College of Aeronautics, Nanjing University of Aeronautics and Astronautics, Nanjing 210016, Jiangsu, China

Abstract

Objective Changes in land cover types lead to numerous ecological and environmental issues. For effective resolution of these issues, monitoring changes in land cover is crucial. Numerous studies have explored the use of full-waveform LiDAR for land cover classification. However, its accuracy can diminish with increasing classification categories. Enhancing classification accuracy necessitates the integration of auxiliary features with waveform features. Research indicates that combining waveform features with the spectral features of optical images can enhance the precision of land cover classification. Given the broad distribution of GEDI data across Earth's surface, it is valuable to investigate if merging GEDI waveform features with optical image spectral features positively impacts land cover classification. Improved accuracy could expand training/validation samples, particularly in regions with limited field surveys or high-resolution remote sensing data. This could enrich the sample pool for land cover classification tasks, thereby boosting overall classification accuracy.

Methods A support vector machine (SVM) was used to classify footprints. First, the GEDI L2A footprint points in the study area in 2020 were extracted, and survey data were used to label the ground object categories under the footprint points. Simultaneously, the spectral reflectance of Landsat remote sensing images at the footprint points was extracted and the vegetation index was calculated. Second, the waveform information and spectrum at the footprint point were normalized, and the sample data were randomly divided into training and verification datasets. Among them, 70% of the training data were used to train the SVM classification model, and 30% were used to verify its accuracy of the classification model. Next, the feature vectors in the training dataset were input into the SVM classification model, and GridSearchCV was used to search for the penalty coefficient and kernel function of the SVM to obtain the optimal parameters and train the optimal classification model of the footprint points. Subsequently, the producer accuracy (PA), user accuracy (UA), overall accuracy (OA), and Kappa coefficient were calculated using the validation dataset to evaluate the model. Finally, the sample data from the six subregions of the study area were extracted. The classification results for the other regions were predicted based on the data training model for each region, and the adaptability of the method was evaluated.

Results and Discussions The importance of two types of source variables (waveform and spectrum) is calculated by using the experiment of the importance of the general classification model (Fig. 3), and multiple feature groups (Table 6) are set according to the feature source and importance to train the prediction model respectively. The evaluation of the model shows that the overall accuracy of using only one type of feature is less than 82%; however, the OA can reach 90.68% when used together (Table 7–11). This shows that the combination of the spectral characteristics of Landsat spectral data and the waveform data of GEDI full-waveform LiDAR data improves the accuracy of land cover classification. The applicability of the method is tested across six subregions (plains, mountains, and hilly landforms) within the study area. Tables 12 and 13 demonstrate the proposed method's strong applicability. However, during the applicability test, challenges may arise due to the limited sample size and imbalanced data distribution. The model's practicality can be achieved by increasing the number of samples and ensuring a balanced dataset.

Conclusions The spectral characteristics of the Landsat spectral data and waveform data of the GEDI full-waveform LiDAR data can be used to improve the accuracy of land cover classification. The overall accuracy of the combined use of spectral and waveform features is 90.68%, which can be improved by more than 8 percentage points when compared to a single feature. When the spectral characteristics of local objects are similar, the structural information provided by the waveform characteristics plays an important role in distinguishing different land cover types. Similarly, when the same types of objects with different structural characteristics or different types of objects with the same structural characteristics appear, the spectral characteristics play a key role. Additionally, data from six subregions in the dataset are utilized to test the applicability of the test model. The results indicate that the proposed method exhibits good universal applicability. Therefore, the combined use of height and spectral features from the GEDI and Landsat OLI data is beneficial for land cover classification of GEDI footprints.

Key words measurement; Global Ecosystem Dynamics Investigation; support vector machine; land cover classification; Landsat